JAMES | Journal of Advances in Modeling Earth Systems

RESEARCH ARTICLE
10.1029/2018MS001576

Control of Convection in High-Resolution Simulations of Tropical Cyclogenesis

D. J. Raymond[1] **and G. Kilroy**[2]

[1]Physics Department and Climate and Water Consortium, New Mexico Tech, Socorro, NM, USA, [2]Meteorological Institute, Ludwig Maximilians University, Munich, Germany

Key Points:
- The control of convection in simulations of tropical cyclogenesis was diagnosed
- The convective mass flux is governed by thermodynamic factors
- This has application to the treatment of convection in large-scale models

Correspondence to:
D. Raymond,
david.raymond@nmt.edu

Citation:
Raymond, D. J., & Kilroy, G. (2019). Control of convection in high-resolution simulations of tropical cyclogenesis. *Journal of Advances in Modeling Earth Systems*, *11*, 1582–1599. https://doi.org/10.1029/2018MS001576

Received 28 NOV 2018
Accepted 29 APR 2019
Accepted article online 2 MAY 2019
Published online 7 JUN 2019

Abstract Three idealized high-resolution simulations of tropical storm formation from a weak vortex are analyzed. The three simulations include a case using warm rain microphysics, a similar case in which surface friction is omitted, and a case in which ice microphysics is used. The goal is to understand the mechanisms controlling the intensity and distribution of convection in the formation process in each of these cases. Simulations of convection in weak temperature gradient convective models show that a combination of low to middle tropospheric moist convective instability, the saturation fraction or column relative humidity, and the surface moist entropy flux explain a high percentage of the variance in precipitation and lower tropospheric vertical mass flux. Tropical cyclones differ from other convective environments in that intense frictional convergence occurs in the boundary layer. Adding a measure of convective inhibition to account for this process enables the lower tropospheric mass flux to be predicted even in the core regions of the simulated tropical cyclones. These results are pertinent to the development of more accurate convective parameterizations for large-scale models.

1. Introduction

Ooyama (1982) synthesized the work of multiple investigators over many years into a coherent picture of tropical cyclone dynamics. His "cooperative intensification" hypothesis forms the basis for our current understanding of tropical cyclone intensification. In this hypothesis, when the developing cyclone acquires sufficient rotation through a deep layer (the "primary circulation") to induce a region of low surface pressure, the resulting cyclonic boundary layer flow spirals inward, leading to boundary layer convergence and deep convection in the cyclone core. The convective updraft air exits the cyclone near the top, eventually sinks to the surface as the result of radiative cooling and returns to the inflow, completing the "secondary circulation." Entrainment into the ascending convective flow draws in surrounding free tropospheric air, intensifying the primary circulation by angular momentum conservation, which results in lower free tropospheric pressure in the circulation center. Hydrostatic balance propagates this lower pressure down to the boundary layer, and the secondary circulation itself intensifies. The primary and secondary circulations thus cooperate to strengthen each other.

Ooyama (1982) asserts that this close coupling between primary and secondary circulations is weak for ordinary tropical disturbances. The salient mechanisms for controlling convection in this case were thought by Ooyama to be more thermodynamic in origin. However, Ooyama did not elaborate on the character of these processes.

Contrary to the hypothesis of Ooyama (1982), frictional convergence is thought by some to play a significant role in the dynamics of convection in tropical disturbances with relatively modest wind speeds compared with those in mature tropical cyclones. For instance, Kilroy et al. (2017a) found in high-resolution simulations of tropical cyclogenesis that frictional convergence acts from the very beginning of tropical cyclone formation.

On larger scales, Wang and Rui (1990) ascribe a significant role for frictional convergence in tropical waves but Moskowitz and Bretherton (2000) assert that frictional convergence is far too strong in their model. On the other hand, there is evidence that frictional convergence is important in the intertropical convergence zone (ITCZ; Back & Bretherton, 2009a; Stevens et al., 2002). Given that frictional convergence operates in both ITCZs and tropical cyclones, consideration of ITCZs is warranted. Zhang et al. (2004) found a shallow return flow coupled to the cross-equatorial boundary layer flow feeding the East Pacific ITCZ, which most

likely results from frictional convergence in the boundary layer. Raymond et al. (2006) found that this shallow return is limited to cases of weak deep convection. In strong convective cases it disappears. Back and Bretherton (2009a, 2009b) present a general model of boundary layer forcing of convection in which surface friction plays a role and point particularly to the tropical East Pacific where this might be pertinent. However, Raymond et al. (2006) found that precipitation in this region correlates with surface wind speed but not boundary layer convergence, which favors thermodynamic control (via surface heat fluxes) as a governing factor for precipitation in the East Pacific.

The primary control on convection in the cooperative intensification theory is frictional convergence, which governs the upward flow of mass out of the boundary layer. However, cooperative intensification is largely silent as to the behavior of this upward mass flux once it leaves the boundary layer. This leaves open the possibility that frictional convergence in the boundary layer and thermodynamic processes in the free troposphere act independently. Numerical simulations by Smith and Wang (2018) support this hypothesis.

Following this thought, we hypothesize that thermodynamic factors control the convective vertical mass flux in the free troposphere independent of frictional convergence in the boundary layer. If free tropospheric mass fluxes exceed the supply from frictional convergence, then additional mass must be drawn in from above the boundary layer. If the reverse occurs, then the excess boundary layer mass flux must exit the system in a shallow flow just above the boundary layer. Kilroy et al. (2016) found in idealized simulations that the ratio of the mass flux at 6 km to that at 1.5 km exceeds unity for developing systems and is less than unity for the decaying case, which supports the above hypothesis. Furthermore, this hypothesis is consistent with the above-noted observations of shallow return flows with weak deep convection in the tropical East Pacific.

Raymond et al. (2015) proposed a theory for the thermodynamic control of convection. In this theory, the statistical behavior of convection is governed by the characteristics of the convective environment. Weak temperature gradient cloud modeling (Raymond & Sessions, 2007; Raymond & Flores, 2016; Sessions et al., 2015) and observations in tropical weather disturbances (Gjorgjievska & Raymond, 2014; Juračić & Raymond, 2016; Raymond & López-Carrillo, 2011; Raymond et al., 2011, 2014, 2017) provide support for this theory. Environmental factors found to control the statistical properties of convection include the column relative humidity or saturation fraction, the low to middle tropospheric moist convective instability, and the surface moist entropy flux. Increasing the saturation fraction and the entropy flux tends to increase the average precipitation rate, while, counter intuitively, increased instability tends to decrease precipitation.

In this paper, we examine the effects of thermodynamic forcing, frictional convergence, and the difference between warm rain and ice physics on convection in idealized high-resolution simulations of tropical cyclone formation by Kilroy et al. (2017a, 2017b) and Kilroy et al. (2018). Ice processes affect convection via the latent heat of freezing induced above the freezing level. In addition, graupel and aggregates of snowflakes can have broadly differing fall speeds, with the latter undergoing rapid melting at the freezing level. These simulations present a broad range of conditions in which convection occurs. In order to avoid entanglement in the detailed dynamics of the tropical cyclone eyewall, thermodynamic processes in two control volumes are considered, one in a circular region within 50 km of the center of the simulated storm (central core), which completely contains the eyewall when it forms, and another in a ring ranging from 50 to 100 km in radius (outer ring). The latter contains much of the convection associated with the outer rainbands.

As long as boundary layer winds are not too strong, the upward velocity at the top of the boundary layer due to frictional convergence is generally much smaller than typical convective vertical motions. However, this upward motion is typically widespread, whereas convection normally covers a small fractional area. This suggests that frictionally induced upward motion acts indirectly on convection via its alteration of the thermodynamic environment, most likely by increasing or decreasing the boundary layer convective inhibition. The addition of a measure of convective inhibition may therefore be sufficient to account for the thermodynamic effects of frictional convergence on deep convection in a tropical cyclone, at least outside of strong eyewalls.

Given this consideration and following the results of Raymond and Flores (2016), we attempt to characterize the lower tropospheric mass flux (averaged over the vertical interval [3, 5] km) in each control volume in terms of the low to middle tropospheric moist convective instability, the column relative humidity or saturation fraction, the surface moist entropy flux, and a measure of convective inhibition. The mass flux in this layer was shown by Raymond et al. (2015) to be an excellent proxy for the average precipitation rate.

Regression methods are used to determine how well the theory of convective control presented by Raymond et al. (2014, 2015) and Raymond and Flores (2016) predicts the lower tropospheric mass flux, given the above parameters. (Note that the term "predict" in this paper is used in the above sense as predictions of a theory rather than as predictions of future behavior.)

Section 2 presents analysis tools used, while simulation results are described in section 3. A detailed analysis of these results is presented in section 4, and conclusions are drawn in section 5.

2. Diagnostic Tools

Raymond and Sessions (2007), Sessions et al. (2015), and Raymond and Flores (2016) showed in weak temperature gradient cloud modeling studies that the rainfall rate is a function of three variables over tropical oceans, the surface moist entropy flux S, the saturation fraction SF, and the instability index II.

The surface moist entropy flux is calculated using a bulk flux formula:

$$S = \rho_s C_K U (s^*_{ss} - s_s), \tag{1}$$

where ρ_s is the air density at the lowest model level, $C_K = 1.29 \times 10^{-3}$ is the assumed surface entropy transfer coefficient, s_s is the moist entropy at the lowest model level, s^*_{ss} is the saturated sea surface moist entropy, and

$$U = (|\boldsymbol{v}_s|^2 + W^2)^{1/2} \tag{2}$$

is the effective wind with a gustiness correction $W = 3$ m/s (Miller et al., 1992), where v_s is the surface wind vector.

The saturation fraction is a kind of column relative humidity:

$$SF = \frac{< \rho r >}{< \rho r^* >} \tag{3}$$

where ρ is the air density, r is the vapor mixing ratio, r^* is the saturated mixing ratio, and angle brackets indicate integration in height z over the troposphere.

The instability index is defined

$$II = s^*_{lo} - s^*_{hi} \tag{4}$$

where s^* is the saturated moist entropy. The subscript *lo* indicates averaging over the vertical interval [1, 3] km while *hi* corresponds to averaging over [5, 7] km. The instability index is a measure of low to middle tropospheric moist convective instability; neutral stability yields $II = 0$. As one might expect, stronger surface fluxes and higher humidity promote stronger convection and more precipitation. However, smaller (but still positive) values of instability index are related to stronger convection. Exactly why this occurs is not completely clear, but it is found in both modeling results (Raymond & Sessions, 2007; Raymond & Flores, 2016; Sessions et al., 2015) and in observations (Raymond et al., 2014).

The discussion in section 1 suggests that a measure of convective inhibition should be added to the list of potential thermodynamic controls of convection. Raymond et al. (2003) and Raymond (2017) showed that an index called *DCIN* (deep convective inhibition) is appropriate for deep convection. Raymond et al. (2003) found that deep convection typically draws on a deeper layer of unstable air, usually assumed to be about 1 km deep, with its ascent inhibited by a stable layer in the 1- to 2-km height range. We therefore define *DCIN* to be

$$DCIN = s^*_{\mathrm{th}} - s_{\mathrm{bl}}, \tag{5}$$

where s^*_{th} is the saturated moist entropy averaged over the [1.2, 1.5] km layer and s_{bl} is the moist entropy averaged over the lowest kilometer. Positive values of *DCIN* are indicative of negative parcel buoyancy just above the boundary layer and hence convective inhibition. Negative values indicate the lack of such an inhibiting layer. (Different versions of *DCIN* use somewhat different averaging intervals.) Raymond and Flores (2016) were able to ignore the effects of *DCIN* since long-term averages were taken in this modeling work. Convective inhibition evolves rapidly in the tropical oceanic boundary layer due to the effects of surface heat fluxes, as indicated by Raymond (1995) and others. However, in the present work, which considers changes over relatively short time intervals, convective inhibition may be important.

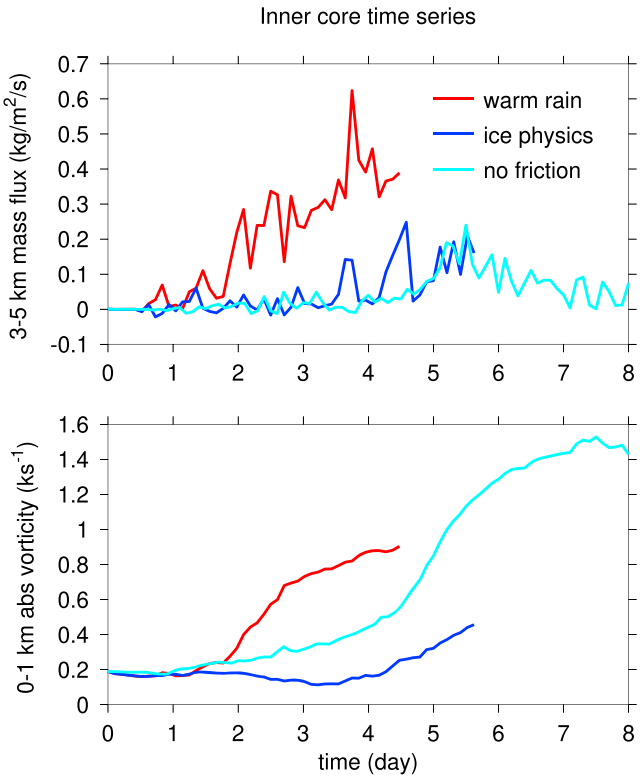

Figure 1. Time series of inner core vertical mass flux averaged over the height interval [3, 5] km and absolute vorticity averaged over [0, 1] km for the three simulations.

In heavy precipitation, saturation fraction and instability index are not independent of each other. By a cloud physical process outlined by Singh and O'Gorman (2013), the two quantities are strongly anticorrelated under these conditions. This occurs because clouds in environments with low humidity need large convective instability to survive entrainment of environmental air, while less instability is needed for moist environments. Clouds in insufficiently unstable environments decay and moisten the environment, whereas those with an excess of instability produce heavy rain, thus drying the environment. Therefore, the clouds themselves drive the environment toward an optimal humidity profile, given the temperature profile. We refer to the tendency for this anticorrelation to develop as "moisture quasi-equilibrium." As the temperature profile relaxes toward the dynamically balanced profile dictated by the pattern of potential vorticity, convection acts to moisten or dry the atmosphere toward an optimum profile, given the environmental temperature profile. Thus, the potential vorticity governs the environmental temperature profile, which in turn controls the humidity profile with the aid of convection.

The heaviest precipitation occurs in regions with the smallest low to middle tropospheric instability and highest column relative humidity (Raymond & Sessions, 2007; Sessions et al., 2015). The instability index tends to decrease in the presence of a strong midlevel vortex, or at least, a deep layer of positive vorticity. The strong vorticity (and hence potential vorticity) results in a more stable temperature profile. The development of strong midlevel vorticity is thus hypothesized by Raymond et al. (2014) as a key step in tropical cyclogenesis.

3. Simulations

Three runs are considered, a case with warm rain cloud physics and surface friction turned on, a second similar to the first but with no surface friction, and a third with surface friction but with a full treatment of ice phase cloud physics (Kilroy et al., 2017a, 2017b, 2018). The simulations are run on a 3,000-km by 3,000-km domain with a horizontally stretched grid. The grid is also stretched in the vertical with 50-m resolution near the surface and 40 vertical levels, extending to 25 km. A simple relaxation model for radiative cooling is employed. The simulations are initialized with an axially symmetric vortex and a composite sounding from the 12 September 2010 observations of the precursor to Atlantic Hurricane Karl using the National Center for Atmospheric Research/National Science Foundation Gulfstream-V aircraft dropsondes (Montgomery et al., 2012). The initial, weakly warm-core vortex has a maximum wind of 5 m/s at a radius of 100 km at the surface, gradually decreasing in strength with height. The focus of our analysis is on the 300-km by 300-km subdomain where the horizontal grid spacing is 0.5 km. Averages are taken over two regions, a domain-centered "inner core" with radius $r < 50$ km and a concentric "outer ring" with $50 < r < 100$ km. Both of these regions are inside the radius of maximum winds of the initial circulation.

Figure 1 shows a time series of the lower tropospheric vertical mass flux and the near-surface absolute vorticity in the inner core for the three simulations. The vorticity and the mass flux tend to change in lockstep for the warm rain and ice cloud physics cases. However, the vorticity of the no-friction case increases to a much greater degree relative to the mass flux than for the other two cases. This is evidently due to the lack of a frictional spin-down tendency in the no-friction case.

All data presented below have been smoothed in time with a 0.5-day low-pass filter unless otherwise indicated. This removes fluctuations induced by the chaotic nature of convection and allows the longer-term trends in the data to be discerned.

3.1. Warm Rain

The warm rain simulation was run for 4.5 days, starting with the previously described initialization. Figure 2 shows the spatially averaged vorticity and vertical mass flux in the inner core region as a function of time and

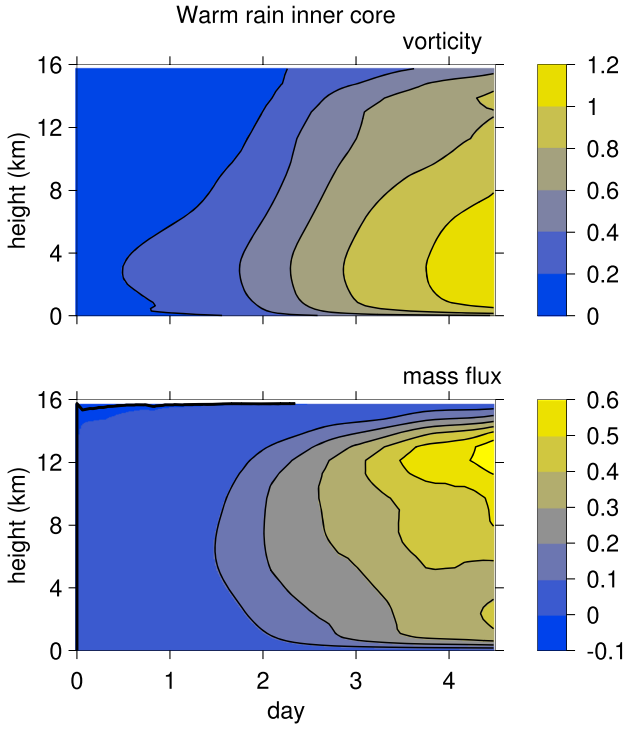

Figure 2. Mean absolute vorticity (ks^{-1}; upper panel) and vertical mass flux ($kg{\cdot}m^{-2}{\cdot}s^{-1}$; lower panel) in the inner core as a function of day and altitude for the warm rain simulation. Heavy contours indicate zero values.

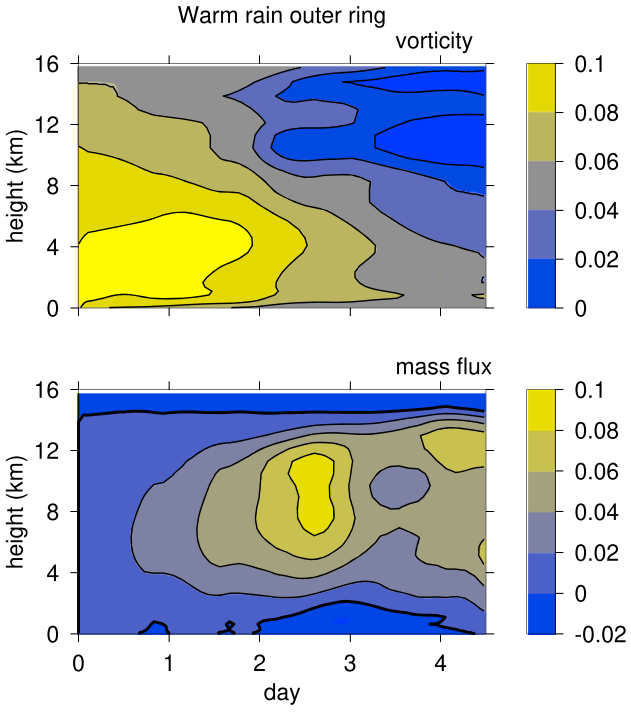

Figure 3. As in Figure 2 except for the outer ring of the warm rain simulation.

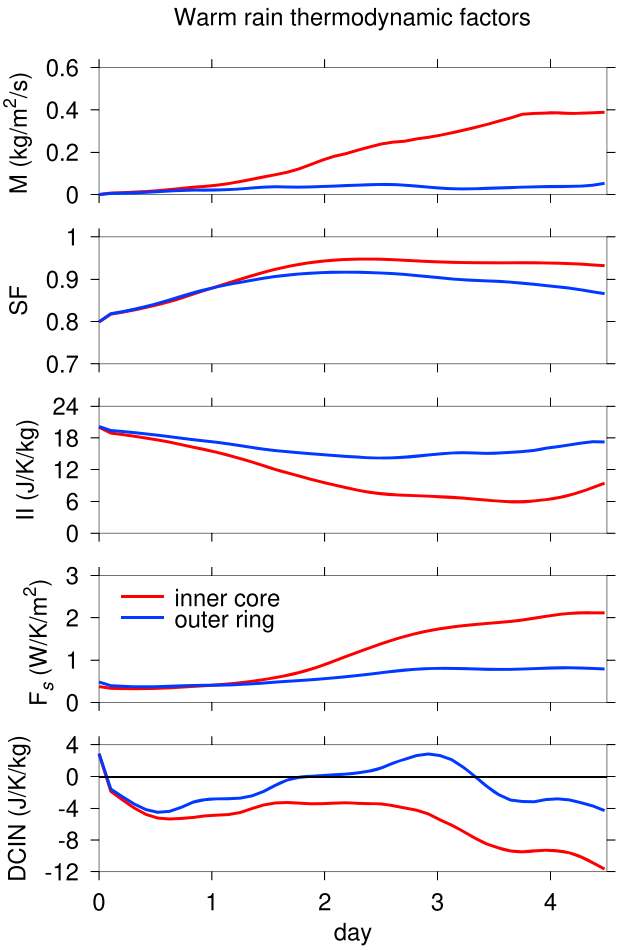

Figure 4. Time series of vertical mass flux averaged over [3, 5] km (M, top panel), saturation fraction (SF, second panel), instability index (II, third panel), surface moist entropy flux (F_s, fourth panel), and convective inhibition ($DCIN$, bottom panel) for the inner core (red) and the outer ring (blue) of the warm rain simulation.

height. Unlike many tropical cyclones in the real world (Raymond et al., 2014), the simulation immediately produces a strong warm core, indicated by the rapid development of a low-level inner core vortex with a broad vorticity maximum between 1 and 5 km. This is consistent with the initial vertical mass flux profile, which is fed by convergence occurring mainly below 5 km. The rapid increase of the mass flux with height below 1 km also implies intense frictional convergence in the boundary layer. After approximately 3 days, nearly uniform convergence extends from 1 to 12 km, which is associated with the entrainment of free tropospheric air and spin-up of the cyclone above the boundary layer.

Figure 3 shows the average vorticity and vertical mass flux in the outer ring region as a function of time and height. In contrast to the inner core, the vorticity in the outer ring decreases with time after a short period (< 1 day) of spin-up in the lower troposphere. Though positive stretching is implied by the mass flux profile in the lower troposphere, inward flow in the presence of a negative radial gradient of vorticity overcomes this positive tendency, resulting in spin-down. In the upper troposphere, negative stretching plus the outward advection of low vorticity air from the upper part of the inner core are largely responsible for the decreasing vorticity in the upper levels of the outer ring.

Time series of various thermodynamic indicators in the inner core and the outer ring yield additional insight into the simulated tropical cyclone and its convection. Figure 4 shows the development of the lower tropospheric vertical mass flux, saturation fraction, the instability index, the surface moist entropy flux, and the $DCIN$ in these two regions. The core vertical mass flux increases monotonically, while the outer ring mass flux oscillates about a much smaller value. The saturation fraction and surface entropy flux increase while the instability index decreases in the first 2 days, which favors deep convection. The changes are more pronounced in the inner core relative to the outer ring. The $DCIN$ decreases equally in the two regions for the first 0.5 day and then undergoes a series of fluctuations. However, inner core convection shows less convective inhibition than the outer ring after 0.5 day. Thus, all thermodynamic control parameters favor the inner core over the outer ring, with this bias increasing through most of the simulation.

3.2. No Friction

This simulation is identical to the warm rain case but with the surface friction turned off. The result is a very different form of cyclone spin-up. The cyclone develops more slowly than in the case with friction, so the integration is extended to 8 days. Figures 5 and 6 show, respectively, the absolute vorticity and vertical mass flux as a function of time and elevation in the inner core and the outer ring. As reported by Kilroy et al. (2017b), the initial spin-up occurs outside of the inner core, with vorticity developing in the low to middle troposphere of the outer ring. This vorticity decreases after 4 days as the inner core ingests vorticity from the outer ring during its spin-up. As occurs in the warm rain case, the vorticity in the upper troposphere of the outer ring decreases with time. The inner core in the no-friction case spins up at about half the rate of the warm rain case with friction and the vorticity structure is very different, with maximum vorticity at the surface. The ultimate vorticity in the core is also significantly stronger than that in the warm rain simulation. In the inner core, the main spurt of convection occurs between 4.5 and 6 days, which is consistent with the increase in the vorticity. Most convergence occurs below 8 km, which is consistent with the vertical distribution of vorticity in the inner core. As expected, there is no evidence of frictional convergence in the mass flux profile. As with the warm rain case, outer ring vorticity peaks just before the intensification of the inner core vortex and then decreases as outer ring vorticity is drawn into the core.

The time series of thermodynamic factors for this case (Figure 7) provides additional insight. The lower tropospheric vertical mass flux is much weaker in the inner core than in the warm rain case and actually

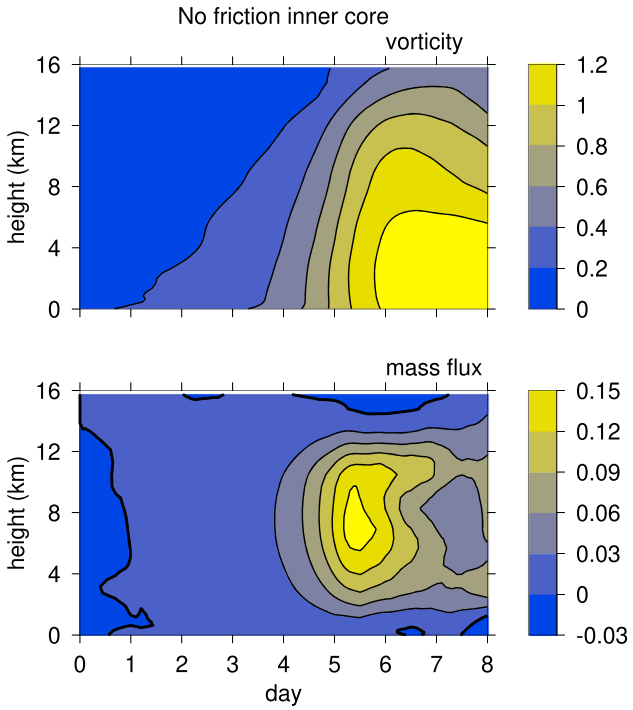

Figure 5. As in Figure 2 except the no-friction simulation.

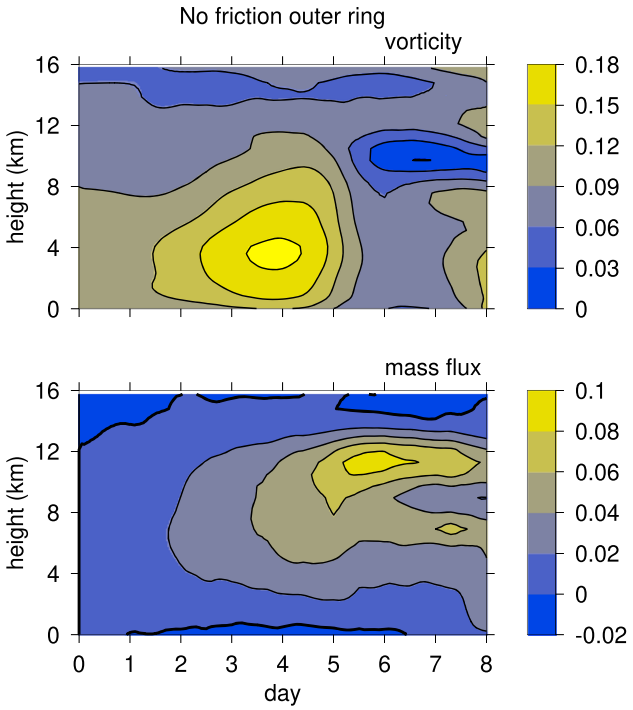

Figure 6. As in Figure 3 except the no-friction simulation.

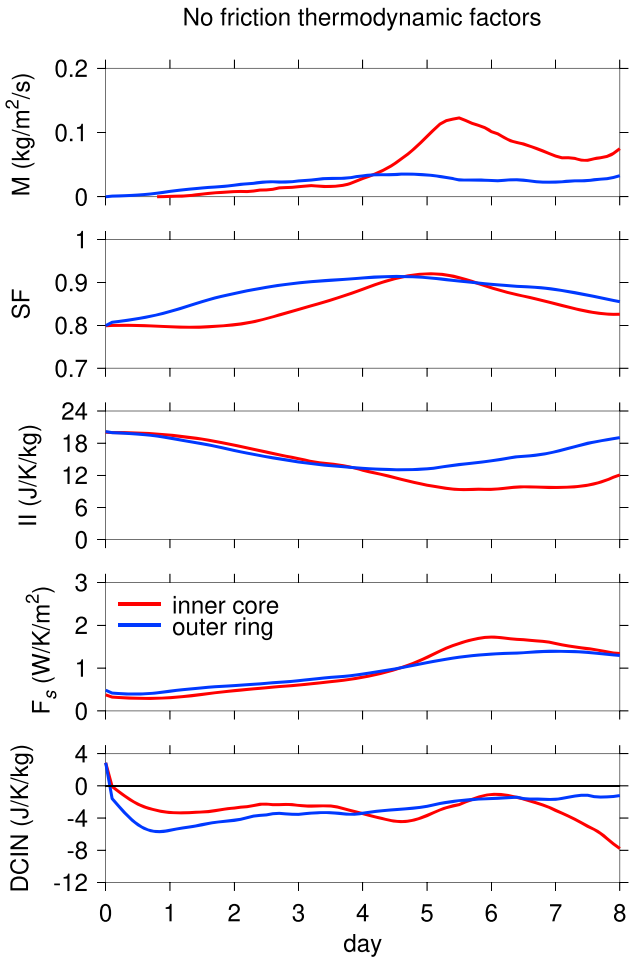

Figure 7. As in Figure 4 except for no-friction case. Note the modified vertical mass flux scale in the upper panel.

decreases in magnitude after 5.5 days. This weakness is evidence that the strength of inner core upward motion is coupled to the existence of frictional convergence there. Notice that the outer ring immediately develops a more negative value of *DCIN* than the inner core. As the initial values of saturation fraction and instability index in the two regions are identical, this can be attributed to the stronger surface moist entropy fluxes in the outer ring, due to the stronger near-surface winds there.

Since little convection develops in the inner core in the first 2 days, the inner core saturation fraction changes little during this period. In contrast, the outer ring saturation fraction begins increasing immediately from the start of the simulation, which gives the outer ring convection a head start. However, the inner core convective mass flux catches up to and surpasses that in the outer ring near 4 days.

3.3. Ice Cloud Physics

Kilroy et al. (2018) describes a simulation in which warm rain physics are replaced by a full cloud physical model including ice processes. The cyclone in this case also develops more slowly than in the warm rain model, so the integration time is slightly extended to about 5.6 days.

Figure 8 shows the inner core vorticity and vertical mass flux as a function of time and height for the ice cloud physics case. The maximum in the vorticity is consistently near an elevation of 5 km, which is higher than in both the warm rain and no-friction cases. This is consistent with the form of the inner core mass flux profile, which exhibits convergence up to 10–12 km from the beginning of cyclone intensification. The rate of development is less than for the warm rain case and comparable to the no-friction case. The outer ring vorticity (Figure 9) increases with time until 4 days and then decreases, in spite of continuing outer ring convection.

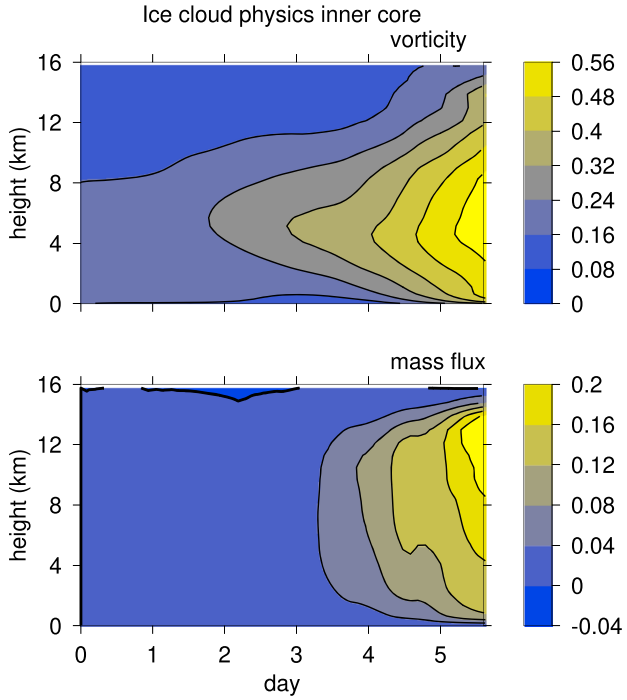

Figure 8. As in Figure 2 except the ice cloud physics simulation.

As Figure 10 shows, the thermodynamic conditions differ only modestly between the inner core and outer ring for roughly the first 2 days. This is consistent with the near equality of the early stage mass flux profiles between these regions. After that, inner core mass fluxes exceed those in the outer ring, probably as a result of a decrease in instability index in the core.

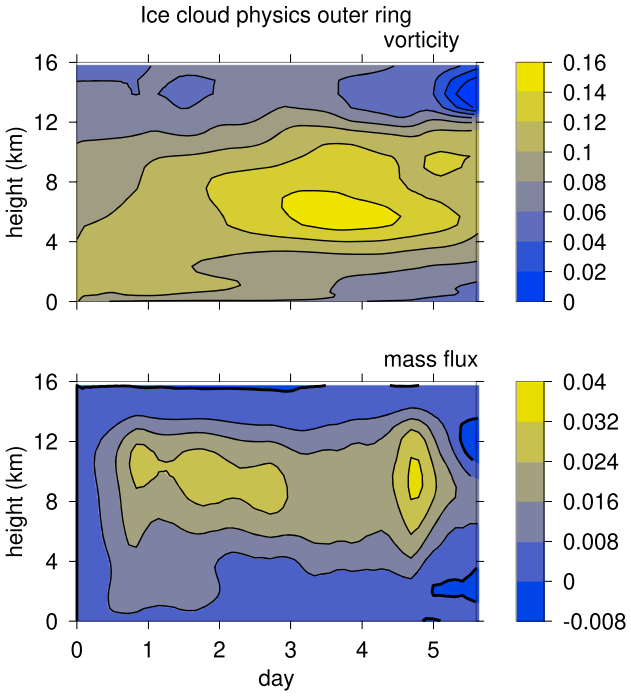

Figure 9. As in Figure 3 except the ice cloud physics simulation.

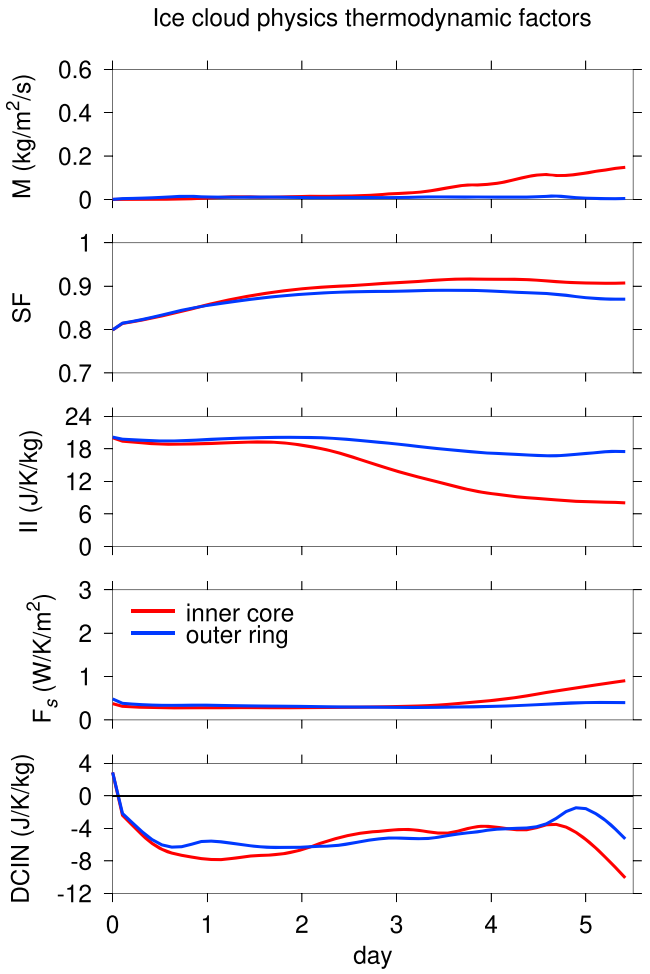

Figure 10. As in Figure 4 except for the ice cloud physics case.

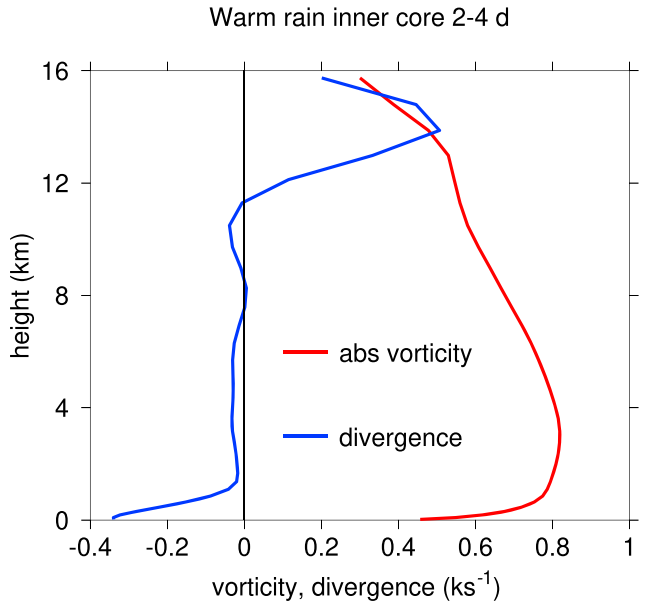

Figure 11. Vertical profiles of absolute vorticity and divergence averaged over the time interval [2, 4] days in the inner core of the warm rain simulation.

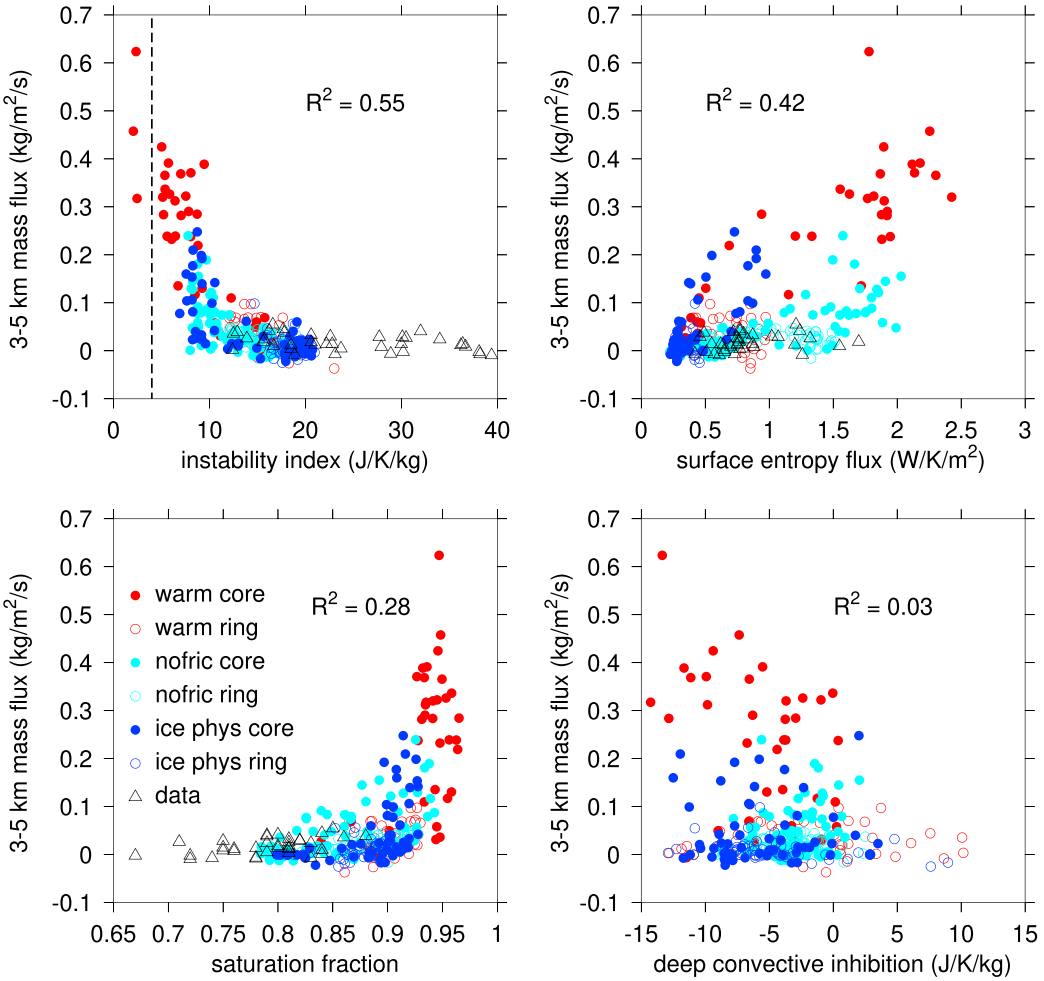

Figure 12. Scatter plots of the instability index (upper left), surface moist entropy flux (upper right), saturation fraction (lower left), and deep convective inhibition (lower right) against the [3, 5]-km average vertical mass flux. Each point represents an average over either the inner core or the outer ring at a particular time. The averaging regions and simulations are distinguished by filled (core) or unfilled (ring) circles of different colors, as indicated. Black triangles indicate observational results as discussed in the text. The value of R^2 in each panel represents the fraction of variance explained in a linear regression between the corresponding variable (model data only) and the mass flux. Points to the left of the dashed line in the instability index plot are omitted from the regression calculation.

4. Analysis and Discussion

We now investigate whether the observed characteristics of convection in the above simulations are representable in terms of the thermodynamic environment. In particular, we ask whether the instability index *II*, saturation fraction *SF*, surface moist entropy flux *S*, and *DCIN* are sufficient to predict average convective rainfall. As we do not have rainfall available in the model output, we use instead the lower tropospheric mass flux defined as an average over the height interval [3, 5] km, as discussed in section 1.

A key requirement for the applicability of the theory of Raymond et al. (2014, 2015) is that the time scale for the evolution of vorticity under the influence of convection be longer than the relaxation time scale to a balanced state. The former equals the inverse of the mean divergence, whereas the latter scales with the inverse of the absolute vorticity. Figure 11 shows that the magnitude of the mean divergence in the inner core over the rapid intensification phase of the warm rain case is much less than the absolute vorticity except in the boundary layer and the upper level outflow layer. Thus, with the exception of these regions, the criterion for balance is well satisfied. An auxiliary criterion is that the life cycle of a convective cell (≈1 hr) must be much less than the time scale for the evolution of vorticity (≥1 day in the warm rain case), a criterion that

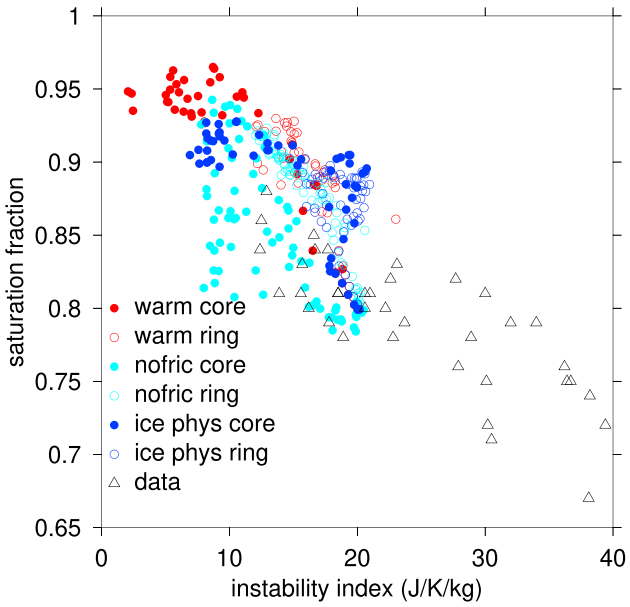

Figure 13. As in Figure 12 except for a scatter plot of instability index versus saturation fraction.

is well satisfied. Since the warm rain case is the most rapidly intensifying, the other cases will also satisfy criteria for balance.

Figure 12 shows scatter plots of the above four thermodynamic variables versus the lower tropospheric mass flux. The inner core ($0 < r < 50$ km) and outer ring ($50 < r < 100$ km) averaging regions for each of the three simulations are represented by symbols with different types and colors in these plots. Observational data from the Tropical Cyclone Structure (TCS08; Elsberry et al., 2008) and the Pre-Depression Investigation of Cloud Systems in the Tropics (PREDICT; Montgomery et al., 2012) experiments (Gjorgjievska & Raymond, 2014) are also shown for the instability index, surface entropy flux, and saturation fraction plots. These data were obtained from horizontal averages of three-dimensional variational analyses of dropsonde observations covering the disturbances in question. (The *DCIN* was not available in this data set.) In general, these observations and the current model results are consistent where overlap occurs, though the observations are biased toward weaker systems.

All four variables are independently correlated to the lower tropospheric mass flux to a certain degree as Figure 12 shows. The correlation between instability index II and mass flux is the strongest (fractional variance explained $R^2 = 0.55$), though the relationship is highly nonlinear. Replacing II by $1/II^2$ straightens out the kink near $II = 10$ J·K^{-1}·kg^{-1}, but the fraction of variance explained is reduced to 0.43. This reduction is the result of the three outlier points with $II < 4$. One can argue on physical grounds for omitting these outliers since they lie close to the $II = 0$ boundary that separates a stable from an unstable environment, a region of phase space that has yet to be explored. Furthermore, they acquire undue importance in the inverse square representation. With this omission, the fraction of variance explained for $1/II^2$ rises to 0.72.

Visual inspection of the lower left panel of Figure 12 shows that the saturation fraction *SF* also has a strong but nonlinear correlation with the lower tropospheric mass flux. Linear regression results in the fractional variance explained of only 0.28. However, representing the effect of saturation fraction by the inverse of the saturation deficit $1/(1 - SF)$, as proposed by Raymond (2000), removes the nonlinearity, with R^2 rising to 0.43. In spite of the moisture quasi-equilibrium relation shown in Figure 13, regressing the instability index against the saturation fraction results in only $R^2 = 0.40$. Regressing $1/II^2$ against $1/(1 - SF)$ improves this to only 0.43. These values are small enough to warrant the inclusion of saturation fraction as a predictor in addition to the instability index.

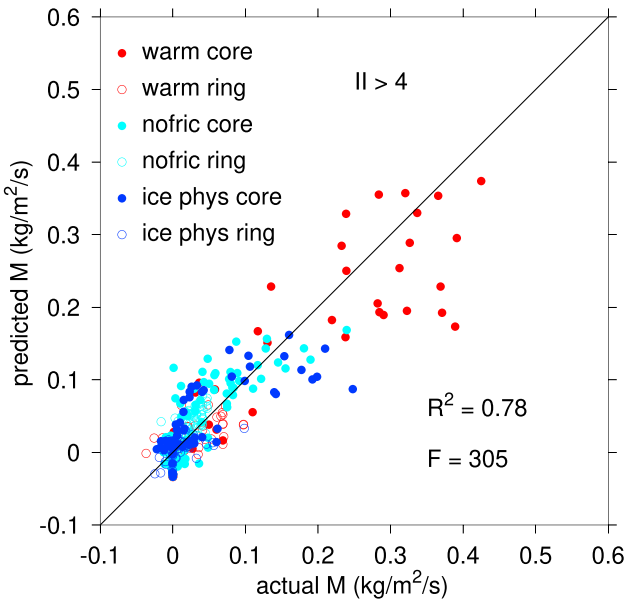

Figure 14. As in Figure 12 except a scatter plot of the actual lower tropospheric ([3, 5] km) mass flux versus the mass flux predicted by a linear superposition of the inverse square of the instability index, the inverse of one minus the saturation fraction, the surface moist entropy flux, and the deep convective inhibition. The superposition coefficients are obtained by linear regression. Cases with $II < 4$ J·K^{-1}·kg^{-1} are omitted.

The surface entropy flux S and mass flux are correlated ($R^2 = 0.42$) and the relationship is largely linear, albeit with a large degree of scatter, as inspection of the upper right panel of Figure 12 shows. S is moderately correlated to instability index ($R^2 = 0.50$) and only weakly correlated to saturation fraction ($R^2 = 0.15$).

The *DCIN* has a very weak correlation with mass flux ($R^2 = 0.03$). However, we include it in the regression for theoretical reasons.

Figure 14 shows the results of a regression with the predicted lower tropospheric vertical mass flux M represented as a linear superposition of $1/II^2$, $1/(1 - SF)$, S, and *DCIN*:

$$M = -0.080 + 6.9/II^2 + 0.0050/(1 - SF) + 0.033S - 0.0028DCIN. \quad (6)$$

The outlier points with values of $II < 4$ J·K^{-1}·kg^{-1} are eliminated from the regression as the magnitude of their influence is amplified by the use of the inverse square formulation. This makes physical sense because such

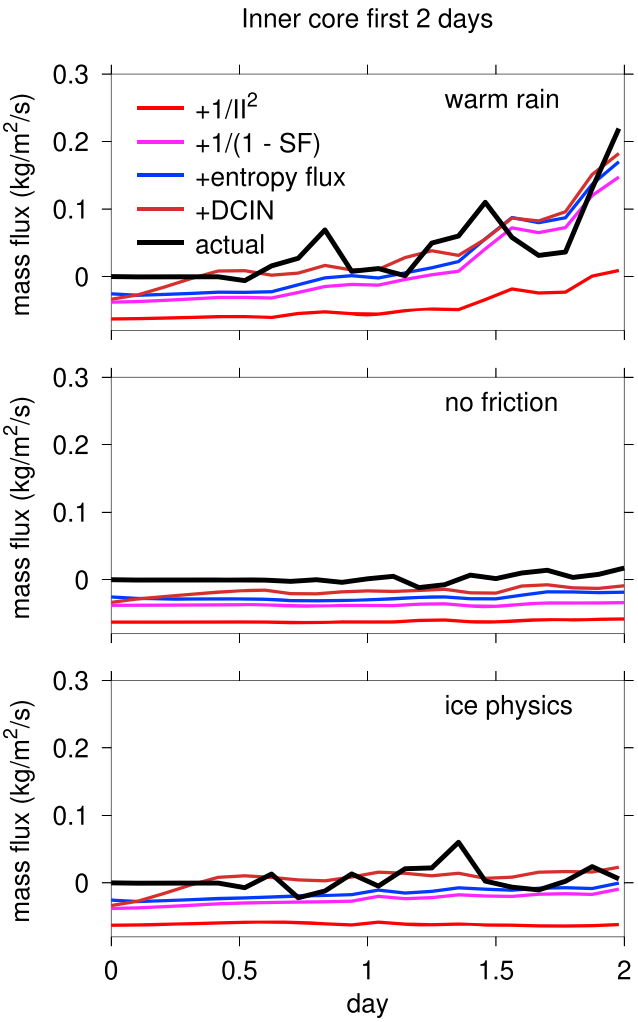

Figure 15. Early evolution (first 2 days) of inner core lower tropospheric mass flux (black lines) and its prediction by 6 (brown lines) for the warm rain (top panel), no friction (middle panel), and ice physics (bottom panel) cases. In each panel the colors red, magenta, blue, and brown represent the partial predicted mass flux resulting from the cumulative addition of the instability index, saturation fraction, surface entropy flux, and deep convective inhibition terms. The horizontal axis is positioned vertically to the value of the constant term in (6). No smoothing in time is applied.

low values of II come close to eliminating the convection completely. The behavior of convection in the limit when $II \rightarrow 0$ remains to be explored.

It is encouraging that the very different inner core and the outer ring regions for the different simulations fall close to the same regression line. Given the vastly different convective regimes in these six different cases, their close correspondence suggests that this result is not spurious. Comparisons with the very different set of simulations of Raymond and Flores (2016) is also enlightening. These simulations were run with a different cloud model in two dimensions and in weak temperature gradient mode. The resulting lower tropospheric mass flux is predicted by the regression ($R^2 = 0.94$) to be

$$M = -0.058 + 5.3/II^2 + 0.0059/(1 - SF) + 0.034S + 0.00057DCIN, \quad (7)$$

which is remarkably close to (6) given the differences between the two cases. (A few outliers with no precipitation or with $II < 4$ J·K^{-1}·kg^{-1} were eliminated from the regression.) The $DCIN$ in this case comes in with the opposite sign from the tropical cyclone simulations but with a magnitude that is insignificant. In fact, excluding $DCIN$ in the regression does not significantly decrease the explained variance in the mass flux, though it does result in minor changes in the three remaining regression coefficients.

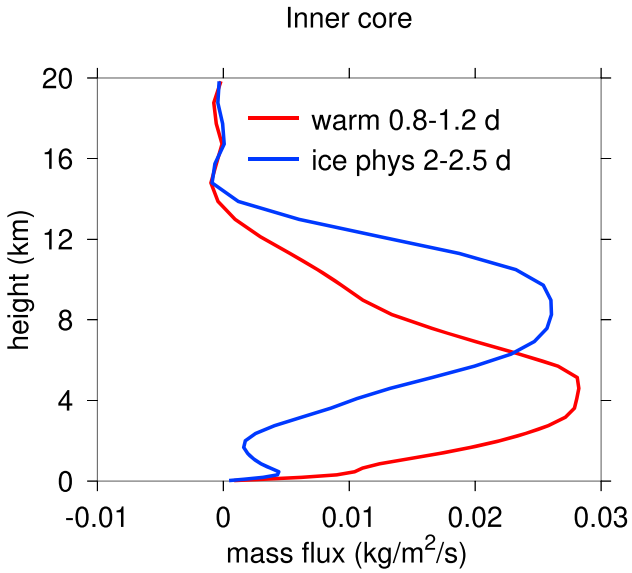

Figure 16. Early stage inner core mass flux profiles for the warm rain and ice microphysics cases.

As is well known, correlation does not necessarily imply causality; the latter requires a plausible physical model to establish a causal relationship. Raymond et al. (2015) argued that inversion of the potential vorticity field yields balanced wind and temperature fields, which in turn control the instability index, the surface moist entropy flux (in conjunction with sea surface temperature and the boundary layer humidity), and the surface momentum. Smith and Montgomery (2008) argue that balanced approximations are inaccurate in the determination of boundary layer winds in tropical cyclones and that the full momentum equations must be used there. However, even in this case, the boundary layer winds depend uniquely on the (balanced) pressure distribution imposed from above, at least in the steady state. For a given instability index, moisture quasi-equilibrium governs the saturation fraction to a certain degree, though shear-induced dry air injection can potentially upset moisture quasi-equilibrium. Absent such effects, the primary circulation in a tropical cyclone and the sea surface temperature therefore appear to govern all the factors that control the lower tropospheric vertical mass flux, at least when averaged over domains with dimensions of order 50 km.

We now use the above results to understand the early stages of tropical cyclogenesis where the pattern is set for subsequent storm development. Each panel in Figure 15 shows the modeled inner core vertical mass flux along with the partial predicted mass fluxes from (6) resulting from the cumulative addition of the instability index, saturation fraction, surface moist entropy flux, and *DCIN* terms in that order. The horizontal axis is positioned vertically to match the constant term in (6). This allows the effects of each term in the predicted mass flux to be inferred.

Though the actual mass flux exhibits oscillations due to the chaotic nature of convection, the total predicted mass flux tracks the actual mass flux with a reasonable degree of fidelity. However, the most striking result is the important role played by the *DCIN* early in the simulations. The *DCIN* decreases rapidly in the first half-day in the warm rain and ice physics simulations and is likely to be responsible for the onset of convection. In the no-friction case, the *DCIN* term does not increase rapidly as frictional convergence is absent in this simulation. Convection in this case is delayed and weak in the first 2 days, strongly suggesting that the initiation of vigorous convection in the inner core depends on the decrease in convective inhibition caused by frictional convergence. This is in agreement with the conclusions drawn by Kilroy et al. (2017a, 2017b).

The increase in the contribution of instability index to the mass flux is much less in the ice physics case than in the warm rain simulation. This is likely the reason that the ice physics case intensifies much more slowly than the warm rain case. Figure 16 shows the vertical mass flux profiles for the warm rain and ice physics cases at comparable stages of development. The ice physics case exhibits a much more top-heavy mass flux profile, implying maximum horizontal mass convergence in the [4, 7]-km range, as opposed to the [0, 3]-km range for the warm rain case. This is consistent with the levels of maximum vorticity for the two cases, as illustrated in Figures 2 and 8.

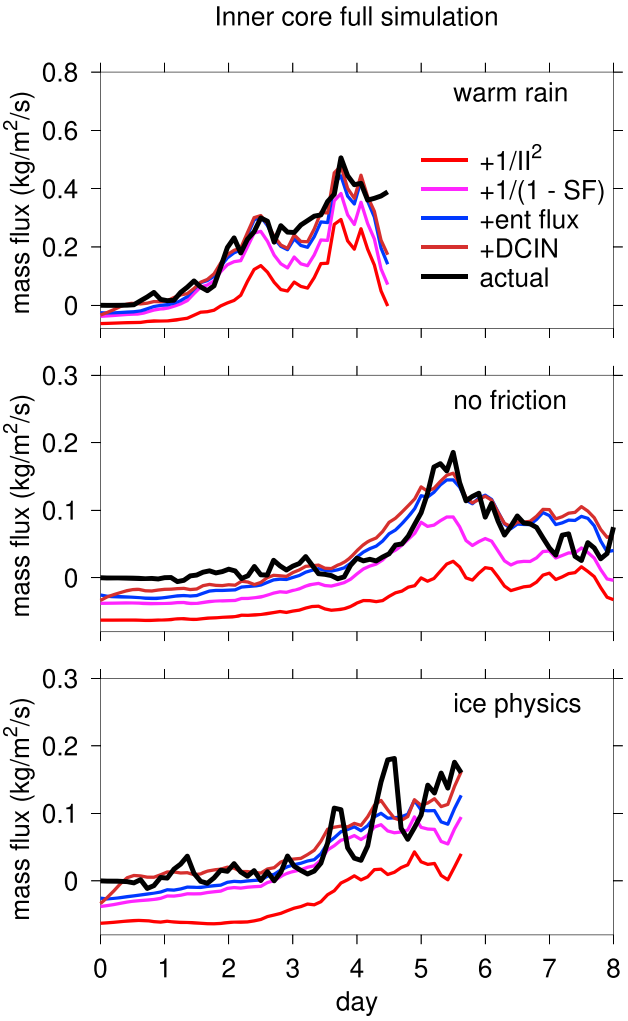

Figure 17. As in Figure 15 except the full evolution of each case is shown. Note the differing vertical scales. Weak smoothing in time with a 0.15-day smoothing length is imposed. The instability index is clipped at a value > 4 $J \cdot K^{-1} \cdot kg^{-1}$, which only affects the warm rain case near 4 days.

Figure 17 shows the full evolution of the three inner core simulation cases in the manner of Figure 15. The full mass flux prediction according to (6) is in reasonable agreement with the actual computed mass flux, as in Figure 15. Figure 18 shows a similar plot for the outer ring. Again, there is reasonable agreement between the modeled and predicted mass fluxes with the exception that the prediction overestimates the mass flux up to approximately 25% near 5 days for the no-friction case.

Curiously, though the *DCIN* is significant in the early phases of the inner core warm rain and ice physics simulations, it becomes much less important as the cyclones intensify. The most important term in the inner core in these two cases is the instability index term (Figure 17). Thus, the stabilization of the inner core environment resulting from the balanced response to the strengthening vortex is central to cyclone intensification in both cases. The saturation fraction term is also important, particularly in the outer ring (Figure 18), indicating the positive effect of column moistening in the core. In both cases with surface friction, the surface entropy flux within the core has a very small effect. This finding appears to be consistent with the results of Montgomery et al. (2009) that capping surface heat fluxes at Trade Wind values reduces the rate of intensification of a simulated tropical cyclone but does not eliminate it. The result is also in contrast to that of Raymond and Flores (2016), where the surface fluxes play a much stronger governing role for convection. Thus, different thermodynamic variables appear to be important in different regimes.

The inner core no-friction simulation exhibits very different behavior. As expected, *DCIN* provides only a small direct contribution to the mass flux throughout the entire simulation. However, the elimination

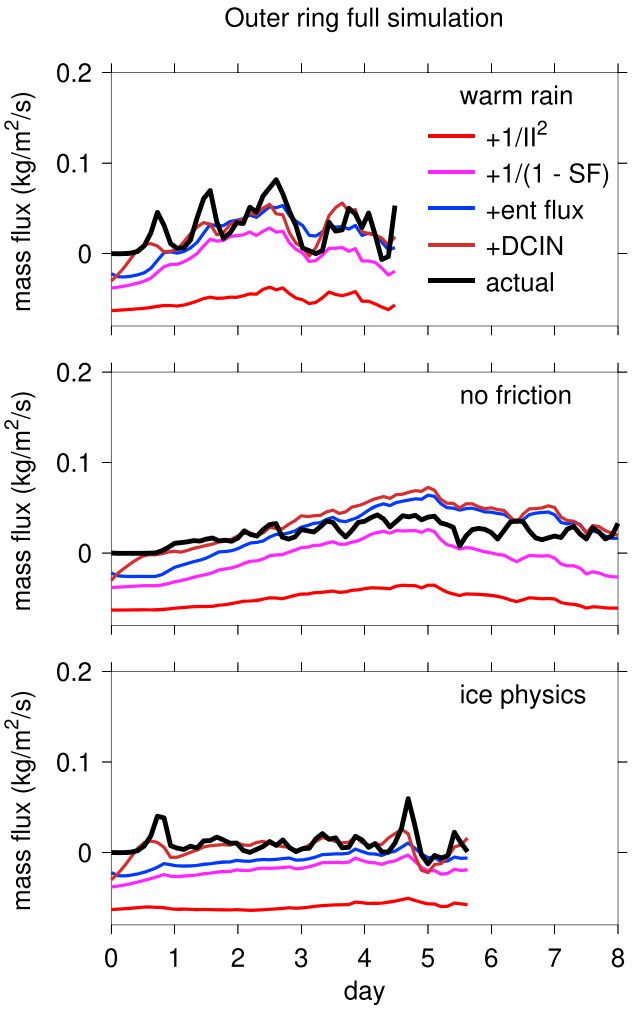

Figure 18. As in Figure 17 except for outer ring.

of frictional convergence drastically reduces the strength of the secondary circulation. This has cascading consequences, starting, perhaps, with the failure of the inner core column to moisten in the first 2 days with consequent detrimental effects on convection.

In the inner core no-friction case the convection weakens after about 5 days. This decrease is accompanied by the development of a strong inversion near 800 hPa (not shown), which appears to be the principal architect of the decay of convection up to the last half-day, at which point the contribution of the instability index term also decreases. A balance develops between the addition of moist entropy by surface fluxes and the export of this entropy by a thin layer of outward flow in the boundary layer (not shown).

The mass fluxes in the outer ring are significantly smaller than inner core values for all simulations with the exception of the first 3 days of the no-friction case. The distribution of forcing components is different as well, with the instability index term playing less of a role in all cases (Figure 18). As in the inner core, the surface moist entropy flux is more important in the no-friction case. Convective inhibition also plays a more significant role in the outer ring of the ice physics case.

5. Conclusions

The central question addressed in this paper is whether thermodynamic factors control deep atmospheric convection in the highly dynamic environment of a tropical cyclone. More specifically, we ask whether the lower tropospheric ([3, 5]-km height-averaged) vertical mass flux can be predicted from the temperature and

humidity profiles plus surface latent and sensible heat fluxes. Analysis of the simulations of Raymond and Flores (2016) shows that this measure of mass flux is tightly related to the precipitation rate per unit area of the convection.

Previous work on less dynamic environments (Raymond & Flores, 2016) indicates that low to middle tropospheric moist convective instability (instability index), the column relative humidity (saturation fraction), and the surface heat flux (represented by the flux of moist entropy) are sufficient in a modeling environment to predict the time-averaged precipitation rate.

The existence of significant frictional convergence in the atmospheric boundary layer suggests that this factor needs to be taken into account as well. The low-level lifting from frictional convergence is weak except in the most extreme circumstances, so its effect is most likely to be felt via lifting-induced modifications to the temperature and humidity profiles at low levels rather than via direct action as a mass supply for deep convection. The convective inhibition encapsulates the effect of these modifications on convection, so a measure of convective inhibition is added to the above list.

The convective inhibition appears to be most important in the earliest stages of convective development in these simulations, when the deep convection is weak. It plays a critical role in getting convection started at that time. However, the instability index is the strongest control on convection in the inner core region once convection has started, with the saturation fraction coming in second. In the outer ring, the instability index is less important relative to the saturation fraction. Though surface heat fluxes constitute the ultimate energy source for tropical cyclones, their direct effect on both inner core and outer ring convection for the warm rain and ice physics simulations is small in these simulations. In the no-friction case, the surface heat fluxes play a much more important role.

It is perhaps surprising that the above four factors are able to explain a rather large fraction of the variance in the lower tropospheric vertical mass flux, and hence precipitation, in both the inner core and outer ring regions of three very different simulations of cyclogenesis. The results also closely match those obtained using the very different modeling environment of Raymond and Flores (2016), suggesting that the results are not accidental but reflect the fundamental physics of deep convection.

This approach could provide a rational basis for the development of more accurate treatments of convection in global atmospheric models. Still to be explored are other aspects of deep convection such as full vertical profiles of the mass flux as well as the profiles of detrained moisture and moist entropy. The extension to a broader range of modeling results as well as real-world data would also be desirable. Nevertheless, the successful use of a small set of thermodynamic parameters to characterize an important aspect of convection over a wide range of environments, including those explored in two different models, suggests that the current approach is promising.

Acknowledgments
Thanks to Roger Smith for many discussions regarding this work. Two anonymous reviewers made perceptive comments which resulted in significant improvements in the paper. Data for this paper are from model runs as cited and are available from Kilroy (gerard.kilroy@lmu.de). Intermediate results are available from Raymond (david.raymond@nmt.edu). Raymond was supported by National Science Foundation Grant 1546698. Kilroy was supported by the Deutsche Forschungsgemeinschaft (German Research Council) under grant KO 2248/2-1.

References

Back, L. E., & Bretherton, C. S. (2009a). On the relationship between SST gradients, boundary layer winds, and convergence over the tropical oceans. *Journal Climate*, *22*, 4182–4196.

Back, L. E., & Bretherton, C. S. (2009b). A simple model of climatological rainfall and vertical motion patterns over the tropical oceans. *Journal Climate*, *22*, 6477–6497.

Elsberry, R. L., & Harr, P. A. (2008). Tropical cyclone structure (TCS08) field experiment science basis, observational platforms, and strategy. *Asia-Pacific Journal of Atmospheric Sciences*, *44*, 209–231.

Gjorgjievska, S., & Raymond, D. J. (2014). Interaction between dynamics and thermodynamics during tropical cyclogenesis. *Atmospheric Chemistry and Physics*, *14*, 3065–3082.

Juračić, A., & Raymond, D. J. (2016). The effects of moist entropy and moisture budgets on tropical cyclone development. *Journal of Geophysical Research: Atmospheres*, *121*, 9458–9473. https://doi.org/10.1002/2016JD025065

Kilroy, G., Montgomery, M. T., & Smith, R. K. (2017b). The role of boundary-layer friction on tropical cyclogenesis and subsequent intensification. *Quarterly Journal of the Royal Meteorological Society*, *143*, 2524–2536.

Kilroy, G., Smith, R. K., & Montgomery, M. T. (2016). Why do model tropical cyclones grow progressively and decay in intensity after reaching maturity? *Journal of the Atmospheric Sciences*, *73*, 487–503.

Kilroy, G., Smith, R. K., & Montgomery, M. T. (2017a). A unified view of tropical cyclogenesis and intensification. *Quarterly Journal of the Royal Meteorological Society*, *143*, 450–462.

Kilroy, G., Smith, R. K., & Montgomery, M. T. (2018). The role of heating and cooling associated with ice processes on tropical cyclogenesis and intensification. *Quarterly Journal of the Royal Meteorological Society*, *144*, 99–114.

Miller, M. J., Beljaars, A. C. M., & Palmer, T. N. (1992). The sensitivity of the ECMWF model to the parameterization of evaporation from the tropical oceans. *Journal Climate*, *5*, 418–434.

Montgomery, M. T., Davis, C., Dunkerton, T., Wang, Z., Velden, C., Torn, R., et al. (2012). The pre-depression investigation of cloud systems in the tropics and PREDICT experiment. *Bulletin of the American Meteorological Society*, *93*, 153–172.

Montgomery, M. T., Sang, N. V., Smith, R. K., & Persing, J. (2009). Do tropical cyclones intensify by WISHE. *Quarterly Journal of the Royal Meteorological Society*, *135*, 1697–1714.

Moskowitz, B. M., & Bretherton, C. S. (2000). An analysis of frictional feedback on a moist equatorial Kelvin mode. *Journal of the Atmospheric Sciences*, *57*, 2188–2206.

Ooyama, K. (1982). Conceptual evolution of the theory and modeling of the tropical cyclone. *Journal of the Meteorological Society of Japan*, *60*, 369–379.

Raymond, D. J. (1995). Regulation of moist convection over the west Pacific warm pool. *Journal of the Atmospheric Sciences*, *52*, 3945–3959.

Raymond, D. J. (2000). Thermodynamic control of tropical rainfall. *Quarterly Journal of the Royal Meteorological Society*, *126*, 889–898.

Raymond, D. J. (2017). Convection in the east Pacific intertropical convergence zone. *Geophysical Research Letters*, *44*, 562–568. https://doi.org/10.1002/2016GL071554

Raymond, D. J., Bretherton, C. S., & Molinari, J. (2006). Dynamics of the intertropical convergence zone of the east Pacific. *Journal of the Atmospheric Sciences*, *63*, 582–597.

Raymond, D. J., & Flores, M. M. (2016). Predicting convective rainfall over tropical oceans from environmental conditions. *Journal of Advances in Modeling Earth Systems*, *8*, 703–718. https://doi.org/10.1002/2015MS000595

Raymond, D. J., Fuchs, Ž., Gjorgjievska, S., & Sessions, S. L. (2015). Balanced dynamics and convection in the tropical troposphere. *Journal of Advances in Modeling Earth Systems*, *7*, 1093–1116. https://doi.org/10.1002/2015MS000467

Raymond, D. J., Gjorgjievska, S., Sessions, S., & Fuchs, Ž. (2014). Tropical cyclogenesis and mid-level vorticity. *Australian Meteorological and Oceanographic Journal*, *64*, 11–25.

Raymond, D. J., & López-Carrillo, C. (2011). The vorticity budget of developing typhoon Nuri 2008. *Atmospheric Chemistry and Physics*, *11*, 147–163.

Raymond, D. J., Raga, G. B., Bretherton, C. S., Molinari, J., López-Carrillo, C., & Fuchs, Ž. (2003). Convective forcing in the intertropical convergence zone of the eastern Pacific. *Journal of the Atmospheric Sciences*, *60*, 2064–2082.

Raymond, D. J., & Sessions, S. L. (2007). Evolution of convection during tropical cyclogenesis. *Geophysical Research Letters*, *34*, L06811. https://doi.org/10.1029/2006GL028607

Raymond, D. J., Sessions, S. L., & López-Carrillo, C. (2011). Thermodynamics of tropical cyclogenesis in the northwest Pacific. *Journal of Geophysical Research*, *116*, D18101. https://doi.org/10.1029/2011JD015624

Sessions, S. L., Herman, M. J., & Sentic, S. (2015). Convective response to changes in the thermodynamic environment in idealized weak temperature gradient simulations. *Journal of Advances in Modeling Earth Systems*, *7*, 712–738. https://doi.org/10.1002/2015MS000446

Singh, M. S., & O'Gorman, P. A. (2013). Influence of entrainment on the thermal stratification in simulations of radiative-convective equilibrium. *Geophysical Research Letters*, *40*, 4398–4403. https://doi.org/10.1002/grl.50796

Smith, R. K., & Montgomery, M. T. (2008). Balanced boundary layers used in hurricane models. *Quarterly Journal of the Royal Meteorological Society*, *134*, 1385–1395.

Smith, R. K., & Wang, S. (2018). Axisymmetric balance dynamics of tropical cyclone intensification. *Quarterly Journal of the Royal Meteorological Society*, *144*, 2350–2357.

Stevens, B., Duan, J., McWilliams, J. C., Munnich, M., & Neelin, J. D. (2002). Entrainment, Rayleigh friction, and boundary layer winds over the tropical Pacific. *Journal Climate*, *15*, 30–44.

Wang, B., & Rui, H. (1990). Dynamics of the coupled moist Kelvin-Rossby wave on an equatorial beta plane. *Journal of the Atmospheric Sciences*, *47*, 397–413.

Zhang, C., McGauley, M., & Bond, N. A. (2004). Shallow meridional circulation in the tropical eastern Pacific. *Journal Climate*, *17*, 133–139.